

# Energy & Environmental Science

Accepted Manuscript

This article can be cited before page numbers have been issued, to do this please use: Z. Song, Q. Huang, Y. Lv, L. Gan and M. Liu, *Energy Environ. Sci.*, 2026, DOI: 10.1039/D6EE02250B.



This is an Accepted Manuscript, which has been through the Royal Society of Chemistry peer review process and has been accepted for publication.

Accepted Manuscripts are published online shortly after acceptance, before technical editing, formatting and proof reading. Using this free service, authors can make their results available to the community, in citable form, before we publish the edited article. We will replace this Accepted Manuscript with the edited and formatted Advance Article as soon as it is available.

You can find more information about Accepted Manuscripts in the [Information for Authors](#).

Please note that technical editing may introduce minor changes to the text and/or graphics, which may alter content. The journal's standard [Terms & Conditions](#) and the [Ethical guidelines](#) still apply. In no event shall the Royal Society of Chemistry be held responsible for any errors or omissions in this Accepted Manuscript or any consequences arising from the use of any information it contains.

## Broader Context

View Article Online  
DOI: 10.1039/D6EE02250B

Aqueous zinc batteries are emerging as a prevalent energy storage system due to resource richness, operational safety, and high capacity of Zn anodes. Benefiting from sustainability, broad structural and functional tunability, aromatic organic materials stand out as promising cathodes for propelling zinc-organic batteries (ZOBs). Organic small molecules with high-density active sites that allow more electron transfer have inspired broad interests as high-capacity cathodes for ZOBs. However, they suffer from high solubility in aqueous electrolytes due to the strong interaction between their polar redox-active motifs and aqueous solvents of electrolytes, triggering irreversible capacity loss after cycling. In this work, we describe nonplanar tertiary-N extended nitrobenzene with stronger intramolecular  $\pi$ - $\pi$  interaction ( $-35.8$  kcal mol $^{-1}$ ) than the dissociation energy of H<sub>2</sub>O (15.1 kcal mol $^{-1}$ ) in aqueous electrolytes. This enables insoluble and low-energy-barrier *N,N,N',N'*-tetrakis(4-nitrophenyl)-1,4-benzenediamine small molecule cathode, which liberates excellent structural anti-dissolution in aqueous electrolytes to afford a state-of-the-art cycling lifespan (180,000 cycles) for ZOBs. Significantly, this nonplanar molecular structure can be further generalized to develop a family of carboxylic, cyano, and imine compounds. This work marks significant progress in discovering insoluble and low-energy-barrier redox-active organic small molecules, which will inspire further efforts to enrich the organic nonplanar structure library in the energy field.



# Nonplanar tertiary-N extended nitrobenzene enables insoluble and low-energy-barrier organic small molecule cathode for high-performance aqueous batteries

View Article Online  
DOI: 10.1039/D6EE02250B

Received 00th January 20xx,  
Accepted 00th January 20xx

DOI: 10.1039/x0xx00000x

Ziyang Song,<sup>a,b,c</sup> Qi Huang,<sup>d</sup> Yaokang Lv,<sup>e</sup> Lihua Gan,<sup>a,c</sup> Mingxian Liu<sup>a,c,\*</sup>

Organic small molecules with a high mass content ratio of redox-active sites are promising high-capacity cathode materials for aqueous zinc batteries, but their strong interaction with aqueous electrolytes causes serious dissolution and limited cycling life. Here we demonstrate nonplanar tertiary-N extended nitrobenzene, which harnesses its strong intramolecular  $\pi$ - $\pi$  interaction beyond the H<sub>2</sub>O dissociation energy, to create an insoluble and low-energy-barrier nitroarene (TNB) small molecule cathode. Two rotating tert-N linkages bring the extended  $\pi$ -aromatic nonplane configuration of TNB, exhibiting a maximum negative intramolecular potential energy of  $-35.8$  kcal mol<sup>-1</sup> compared to its large repulsive force of  $15.1$  kcal mol<sup>-1</sup> in H<sub>2</sub>O medium. Consequently, the intramolecular  $\pi$ - $\pi$  interaction of TNB is significantly stronger than the dissociation energy of H<sub>2</sub>O, which affords structural anti-dissolution in aqueous electrolyte, extending battery lifespan to the state-of-the-art level (180,000 cycles). Meanwhile, the nonplanar structure of TNB allows for 98.9% utilization of nitro/tert-N motifs with low activation energy (0.23 eV), liberating superior capacity (430 mAh g<sup>-1</sup>) and large-current tolerance (100 A g<sup>-1</sup>). Significantly, this nonplanar molecular design shows promising preliminary generalizability to develop versatile insoluble carboxylic, cyano, and imine compounds. These proof-of-concept results suggest a potential paradigm for highly active and ultrastable organic molecules towards better aqueous batteries.

## Introduction

With growing requirement for sustainable and efficient energy storage solutions, rechargeable aqueous batteries have inspired great attention because of high energy supply, operational safety, and natural abundance.<sup>1-5</sup> Currently, aqueous Zn-ion batteries prevail as the leading system, which are highly praised for their low potential ( $-0.76$  V vs. standard hydrogen electrode), high capacity (820 mAh g<sup>-1</sup>), and environmental friendliness of Zn anodes.<sup>6-10</sup> One significant task for the development of Zn batteries is seeking suitable cathode materials.<sup>11-15</sup> Aromatic organic materials (e.g., quinones, azines, azobenzenes, nitroaromatics) possess sustainability, resources sustainability, and customizable functions,<sup>16-21</sup> becoming promising cathode candidates to propel the community of Zn-organic batteries (ZOBs). Featured with high-density redox-active sites,  $\pi$ -aromatic organic small molecules allow more electron transfer, which have captured significant attention as high-capacity cathodes for ZOBs.<sup>22-25</sup> Unfortunately, they are easily dissolved in aqueous electrolytes due to their strong interactions with water solvents, leading to fast capacity loss after cycling.<sup>26-28</sup>

To alleviate the dissolution concern and improve cycling stability of organic small molecules, a prevailing strategy has been implemented, *i.e.*, polymerizing soluble molecules into covalent organic frameworks (COFs) or  $\pi$ -conjugated polymers.<sup>29-33</sup> The first example affords planar  $\pi$ -conjugated skeleton robustness to decrease the solubility in aqueous electrolytes for long-life ZOBs (20,000 cycles).<sup>34</sup> However, this inevitably adds a high proportion of redox-inactive benzene ring nodes to the organic skeleton and/or faces synthesis/purification complexity.<sup>34-36</sup> Another example about the polymers seems to be a feasible method based on the robust solid structure to eliminate the dissolution phenomenon and prolong battery lifespan (10,000 cycles).<sup>37-39</sup> Unfortunately, twisted polymeric chains and random folding structures often bring high spatial reaction energy barriers for built-in redox-active units, limiting the utilization of multi-redox motifs with reduced available capacities ( $<250$  mAh g<sup>-1</sup>).<sup>32,33,40,41</sup> Overall,  $\pi$ -conjugated COFs or polymers face a tricky trade-off between high capacity and long life, leaving large space for structural engineering to strategically reform ZOBs.

To bridge these gaps, exploring insoluble organic small molecules with robust structures and low-energy-barrier functions without compromising their multi-redox capabilities stands as a pivotal objective in pursuing better ZOBs. So far, there are three prevailing solutions to conquer the dissolution issue of organic small molecules for ZOBs: constructing stable intramolecular H-bonds with inert amine donors,<sup>17,42</sup> carbon encapsulation,<sup>13,43</sup> and planar structure extension with benzene rings.<sup>26,44,45</sup> These methods broaden the electrochemical horizons of anti-dissolution organic small molecules, affording long-lasting ZOBs (up to 50,000 cycles). Unfortunately, they often need to integrate high proportion of inactive constituents with high energy barriers, limiting their redox capacity

<sup>a</sup> School of Chemical Science and Engineering, State Key Laboratory of Cardiovascular Diseases and Medical Innovation Center, Shanghai East Hospital, Tongji University, 1239 Siping Road, Shanghai 200092, China. \*E-mail: liumx@tongji.edu.cn

<sup>b</sup> State Key Laboratory of Pollution Control and Resource Reuse, College of Environmental Science and Engineering, Advanced Research Institute, Tongji University, 1239 Siping Road, Shanghai 200092, China.

<sup>c</sup> Shanghai Key Lab of Chemical Assessment and Sustainability, Shanghai 200092, China.

<sup>d</sup> State Key Laboratory of Photovoltaic Science and Technology, Institute of Optoelectronics, College of Future Information Technology, Fudan University, Shanghai 200438, China.

<sup>e</sup> College of Chemical Engineering, Zhejiang University of Technology, 18 Chaowang Road, Hangzhou 310014, China.



(<300 mAh g<sup>-1</sup>) and/or rate performance (<20 A g<sup>-1</sup>). As is well known,  $\pi$ - $\pi$  stacking interaction extensively exists in aromatic organic molecules due to  $\pi$ -electron clouds on benzene rings, which governs their molecular conformation, properties and performances.<sup>46-49</sup> In essence, the insolubility of aromatic molecules implies that their intramolecular  $\pi$ - $\pi$  interactions should be stronger than solvation forces generated by water molecules in aqueous electrolytes. Following this principle, we envision creating nonplanar molecular conformations with extended aromatics into water-insensitive insoluble organic skeletons, which not only form strong intramolecular  $\pi$ - $\pi$  stacking interactions to maintain structural regularity in aqueous electrolytes, but also fully expose redox sites with low spatial energy barriers for multielectron transfer. Consequently, the dissolution concern of organic small molecules should be well solved, thereby propelling ZOBs with dual-high activity and durability, but this has not yet been achieved.

In this work, we report nonplanar tertiary-N extended nitrobenzene with stronger intramolecular  $\pi$ - $\pi$  interaction than the dissociation energy of H<sub>2</sub>O in aqueous electrolytes, which enables insoluble and low-energy-barrier *N,N,N',N'*-tetrakis(4-nitrophenyl)-1,4-benzenediamine (TNB) small molecule cathode for state-of-the-art aqueous ZOBs. Two rotating tert-N linkages bring the extended  $\pi$ -aromatic nonplane configuration of TNB, which shows stronger

intramolecular  $\pi$ - $\pi$  interactions (-35.8 kcal mol<sup>-1</sup>) than H<sub>2</sub>O dissociation forces (15.1 kcal mol<sup>-1</sup>), thus liberating structural insolubility in aqueous electrolytes to afford a state-of-the-art cycling lifespan (180,000 cycles) for ZOBs. Multi-redox TNB with nonplanar structure allows 98.9% utilization of n-p fused nitro/tert-N motifs with a low energy barrier (0.23 eV) *via* co-storing Zn<sup>2+</sup> and SO<sub>4</sub><sup>2-</sup> ions, liberating an ultrahigh capacity and high-rate capability. More importantly, this nonplanar molecular design exhibits encouraging initial generalizability, as further demonstrated by its successful application to carboxylic, cyano, and imine compounds. While additional structural optimization and systematic validation are ongoing, these proof-of-concept results marks significant progress in discovering insoluble and low-energy-barrier redox-active organic small molecules, which will inspire further efforts to enrich the organic nonplanar structure library in the energy field.

## Results and Discussion

Fig. 1a demonstrates the nonplanar molecular engineering of TNB, which integrates dual-electron-acceptor nitro sites of planar 1,4-dinitrobenzene (DB) and single-electron-donating rotated tert-N species of nonplanar triphenylamine (TA) into an extended  $\pi$ -conjugated multi-redox aromatic skeleton (Fig. S1). Generally, due to

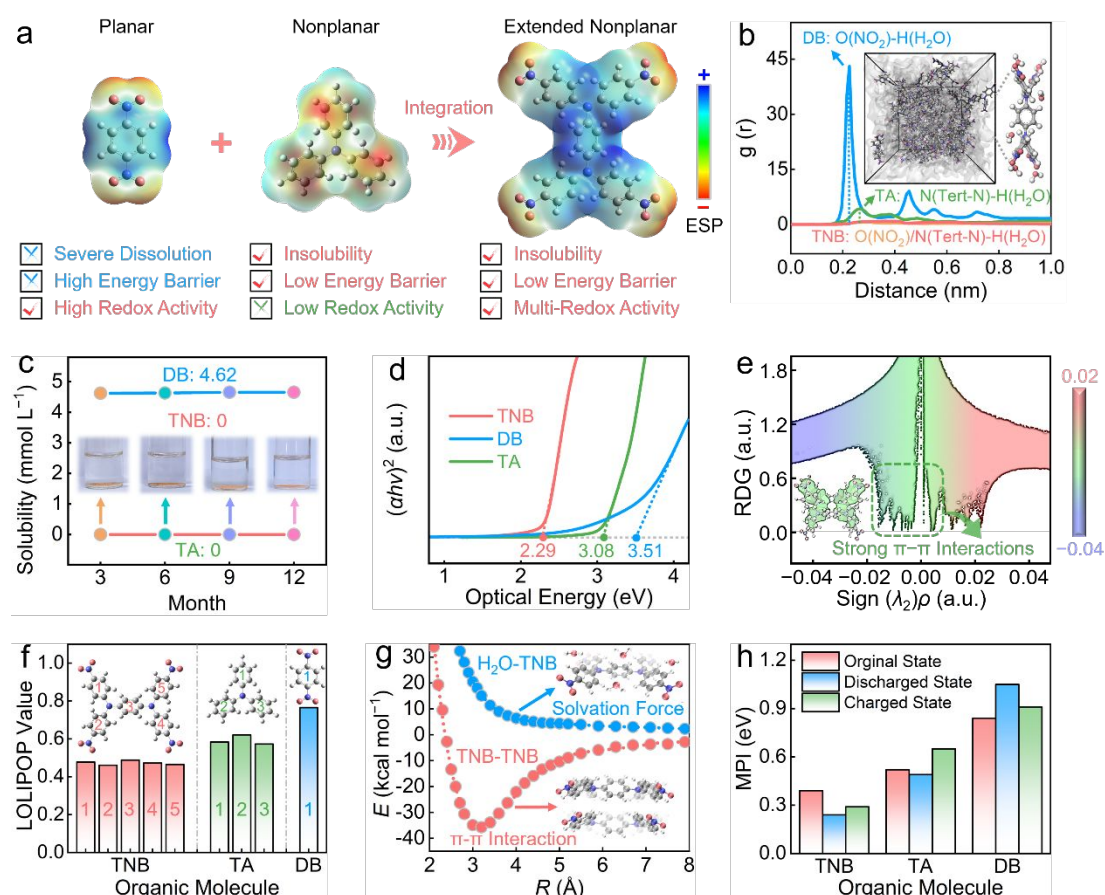


**Fig. 1** Structural analysis of organic small molecules. (a) Molecule structures, ESP maps and electrochemical properties of DB, TA and TNB (grey, blue, red, and white balls represent C, N, O, H atoms, respectively). (b) RDFs of DB, TA and TNB to H<sub>2</sub>O (insert: molecular dynamics simulation snapshots of TNB in 3 M ZnSO<sub>4</sub>/H<sub>2</sub>O solution and corresponding interaction structure between stacked TNB and H<sub>2</sub>O). (c) Solubility and photos of ZnSO<sub>4</sub>/H<sub>2</sub>O solution soaked with DB, TA and TNB for different times. (d) Optical energy gaps of small molecules. (e) RDG scattered points against sign( $\lambda_2$ ) $\rho$  (insert: gradient isosurface). (f) LOLIPOP values. (g) Potential energy profiles for the  $\pi$ - $\pi$  stacked TNB in comparison to interacted H<sub>2</sub>O molecules. (h) Molecular polarity index at different electrochemical states.



the two-electron redox capability of each nitro motif,<sup>50</sup> DB delivers high redox activity to trigger multielectron charge storage. However, its small planar structure faces severe dissolution and high reaction energy barriers in aqueous electrolytes, making it difficult for ionic carriers to utilize its buried electroactive nitro groups.<sup>20</sup> In contrast, the rotated p-type tert-N site generates a nonplanar structure,<sup>51</sup> which is expected to fully expose low-energy-barrier active sites and achieve structural insolubility of TA. Unfortunately, it is trapped by low capacity due to single-electron reactions. Thus, TNB was developed via the nonplanar molecular engineering to leverage the merits of DB (high redox activity) and TA (low energy barrier and insolubility), while compensating for their respective flaws (Fig. 1a).

Nuclear magnetic resonance pattern, Fourier transform infrared (FT-IR) spectra, scanning electron microscopy (SEM) images, and X-ray diffraction (XRD) patterns confirm the structural and functional constituents of TNB (Figs. S1–S5). Molecular electrostatic potential (ESP) simulation,<sup>52,53</sup> was applied to infer the electron structures and redox properties of three organic molecules (Fig. S6a–c and Fig. 1a). On the van der Waals surface of DB, two nitro sites show a more negative ESP value of  $-24.83 \text{ kcal mol}^{-1}$  than the tert-N motif of TA ( $-7.82 \text{ kcal mol}^{-1}$ ), which implies the higher redox activity of DB. In contrast, TNB shows the most negative ESP value of  $-41.87 \text{ kcal mol}^{-1}$ , which makes its redox-sites more accessible to electrons and ions. Specially, four electronegative nitro regions and electropositive tert-N sites of TNB are considered as n-type and p-type motifs for the chelation of cationic and anionic carriers, respectively. It highlights the ambipolar redox attribute of TNB, which delivers the ability to store opposite charges.

To decipher the solubility of three organic molecules in 3 M  $\text{ZnSO}_4/\text{H}_2\text{O}$  electrolyte, molecular dynamics (MD) simulations were conducted.<sup>54,55</sup> The radial distribution functions (RDFs) of DB appear a significant peak of  $\text{O}(\text{NO}_2)\text{-H}(\text{H}_2\text{O})$  at the position range of 0.20–0.30 nm (Fig. 1b), which indicates strong H-bonding interaction between highly redox-active nitro functional groups and water molecules, making it easily soluble in the electrolyte. In contrast, RDFs of TA shows an insignificant peak of  $\text{N}(\text{C-N})\text{-H}(\text{H}_2\text{O})$  at the position of 0.23 nm, implying its negligible interaction with  $\text{H}_2\text{O}$  molecules due to the low electroactivity of the tert-N motif, thus affording structural stability. Of note, there is no response signal in RDFs for TNB, which indicates that it does not interact with  $\text{H}_2\text{O}$  molecules (illustration of Fig. 1b), supporting structural anti-dissolution.

The dissolution behavior of DB, TA and TNB molecules in 3 M  $\text{ZnSO}_4/\text{H}_2\text{O}$  electrolyte after different times of 3–12 months is further studied by ultraviolet-visible (UV-Vis) spectrum analysis. Compared with highly soluble DB ( $4.62 \text{ mmol L}^{-1}$ ), the concentration of TNB was assessed to be  $0 \text{ mmol L}^{-1}$  (Fig. 1c and Fig. S6d–f), which suggests its structural insolubility in aqueous solutions (also reflected by colorless electrolytes, insert of Fig. 1c). Such an excellent anti-dissolution of TNB is attributed to the extended nonplanar  $\pi$ - $\pi$  stacking configuration, which spreads excess charges throughout the skeleton and suppressing the TNB- $\text{H}_2\text{O}$  interaction force to liberate structural robustness, which would promote its stable cycling in aqueous zinc batteries.

The optical energy gap ( $E_g$ ) from solid-state UV/Vis spectra were measured to be 2.29 eV for TNB (Fig. 1d), which is lower than DB (3.51 eV) and TA (3.08 eV), devoting to efficient electron conduction and high-kinetics redox reaction with low energy barriers. The localized orbital locator- $\pi$  (LOL- $\pi$ ) color-filled map,<sup>55</sup> was further performed to unravel the electron structure of TNB (Fig. S7). The extended highly  $\pi$ -conjugated nonplanar aromatic structure endows TNB with higher conductivity than those of DB and TA (Fig. S8), which is beneficial for promoting efficient electron delocalization through the whole skeleton and ensuring structural integrity to suppress dissolution in electrolytes (Fig. S9). It is well-known that the extended  $\pi$ - $\pi$  stacking conjugated structure of organic materials helps to reduce the band gap ( $\Delta E$ ) of the highest occupied molecular orbital (HOMO) and the lowest unoccupied molecular orbital (LUMO).<sup>56–58</sup> Consequently, TNB with an expanded  $\pi$ -conjugated nonplane structure delivers the lowest  $\Delta E$  of 3.09 eV (Fig. S10) in comparison to DB (4.78 eV) and TA (4.23 eV), promising convenient electron injection/removal (Fig. S11).

The reduced density gradient (RDG) analysis,<sup>59,60</sup> was performed to reveal the intramolecular force of TNB (Fig. 1e). The generated strong green spike signals located at  $-0.02\sim 0.02 \text{ a.u.}$  of the  $\text{sign}(\lambda_2)\rho$  denote powerful intramolecular  $\pi$ - $\pi$  interactions derived from the large  $\pi$ -conjugation nonplanar structure (also reflected in the corresponding gradient isosurface map, insert of Fig. 1e). In addition, the  $\pi$ -electron localized orbital locator (LOL- $\pi$ ) integrated  $\pi$  over plane (LOLIPOP) method,<sup>56</sup> as a representative of the strength of  $\pi$ - $\pi$  stacking interactions, was applied to evaluate the  $\pi$ -stacking ability of TNB molecule (Fig. 1f). Theoretically, the smaller the LOLIPOP value of aromatic rings, the stronger the  $\pi$ - $\pi$  stacking interaction. Compared to DB (0.765) and TA (0.584–0.621), different aromatic rings of TNB show the smallest LOLIPOP values (0.461–0.488), indicating its strongest  $\pi$ - $\pi$  stacking intramolecular interactions, which contribute to excellent structural integrity.

Potential energy curves unravel that the intramolecular  $\pi$ - $\pi$  interaction strength of TNB between adjacent nonplanar structures (TNB-TNB) are significantly stronger than the solvation interaction between  $\text{H}_2\text{O}$  molecules and TNB (TNB- $\text{H}_2\text{O}$ ) (Fig. 1g). Particularly, the strong intramolecular  $\pi$ - $\pi$  forces can be reflected by the most negative potential energy ( $E$ ) of  $-35.8 \text{ kcal mol}^{-1}$  at the stacked layer distance ( $R$ ) of 0.32 nm, in comparison to the large repulsive force of  $15.1 \text{ kcal mol}^{-1}$  for TNB- $\text{H}_2\text{O}$ . These results agree with the XRD result (Fig. S5a), of which the diffraction peak at  $27.3^\circ$  and a  $d$ -spacing of 0.32 nm (Fig. S5b) are attributed to typical  $\pi$ - $\pi$  stacking of nonplane structures. Thus, the intramolecular  $\pi$ - $\pi$  interaction is stronger than the solvation force of  $\text{H}_2\text{O}$ , contributing to the structural insolubility of TNB.

Besides, the molecular polarity index (MPI) of DB, TA and TNB molecules was simulated to analyze their solubility during the (dis)charge process (Fig. 1h). The MPI is an indicator for measuring the polarity of organic systems through the features of ESP maps (Fig. 1a). In theory, the larger the MPI, the greater the overall polarity of the molecule and its solubility in  $\text{H}_2\text{O}$  medium.<sup>61</sup> DB molecule at different electrochemical states shows the largest MPI (0.84–1.05) due to the high partial charge and redox activity of nitro sites. TA exhibits reduced MPI (0.49–0.65) derived from the low



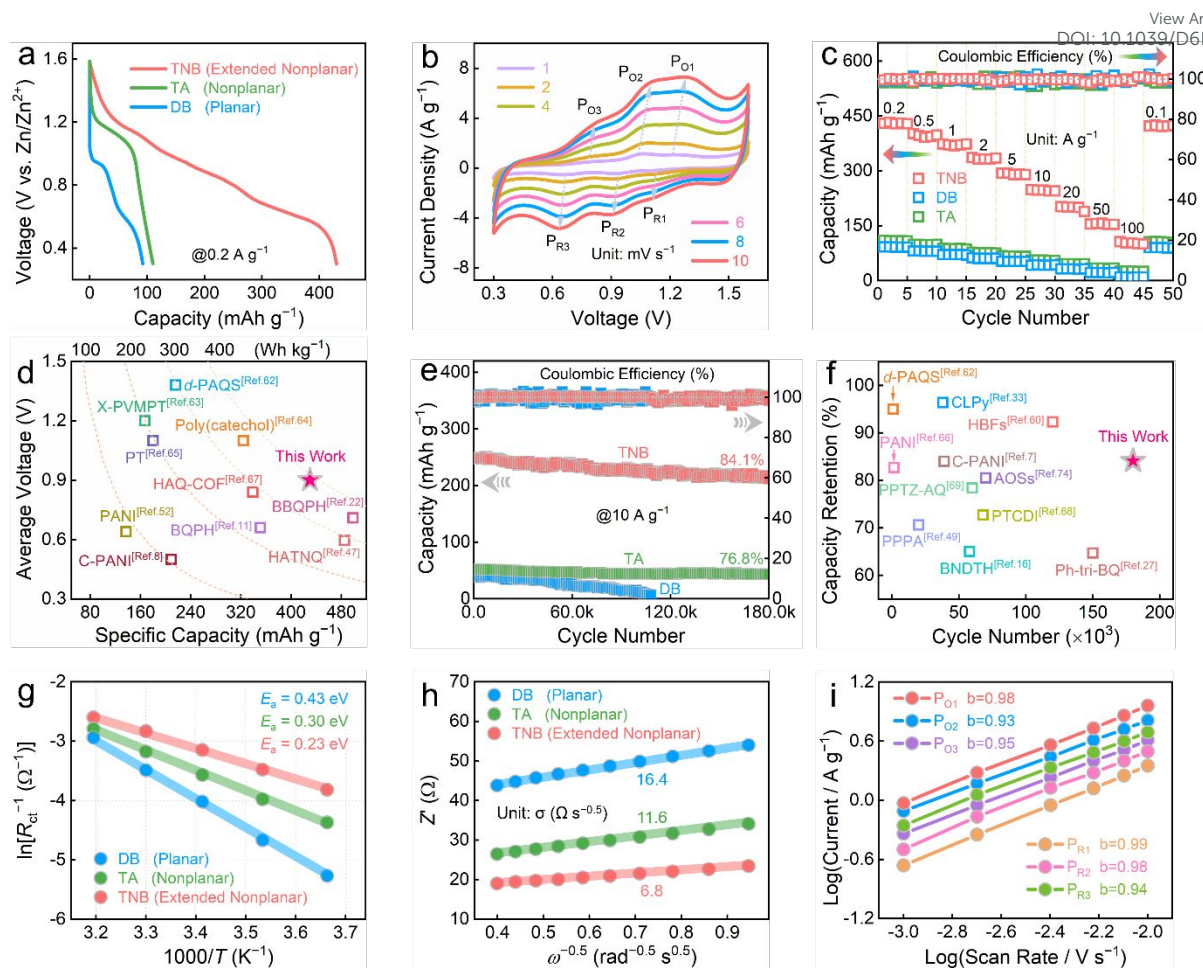


**Fig. 2** Electrochemical performance metrics of TNB cathode. (a) GCD curves of TA, DB and TNB cathodes in ZOBs. (b) CV profiles of Zn||TNB cell. (c) Rate capacities. (d) Capacity-voltage contour map of TNB and previously reported organics used in aqueous batteries. (e) Cycling performance. (f) Life comparison of TNB with reported organics used in aqueous batteries. (g) Evaluated  $E_a$  values and (h)  $\sigma$  values of ionic carriers of TA, DB and TNB cathodes in ZOBs. (i) Evaluated  $b$  values of Zn||TNB battery.

reactivity of tert-N sites. In contrast, the (dis)charge products of TNB molecule liberates the smallest MPI (0.24–0.39) because of the stronger nonplanar  $\pi$ -conjugation effect, and thus the smallest solubility in  $H_2O$  medium, which agrees with the experimental results. Overall, TNB fuses structural insolubility and exposed multi-redox sites with low energy barriers, which are expected to be highly desirable features for activating high-performance ZOBs.

The electrochemical properties of TNB cathode were investigated in ZOBs by using Zn metal anode and 3 M  $ZnSO_4/H_2O$  electrolyte (Figs. S12 and S13). Zn||TNB battery liberates an ultrahigh specific capacity of  $430 \text{ mAh g}^{-1}$  at  $0.2 \text{ A g}^{-1}$  based on galvanostatic (dis)charge (GCD) profiles (Fig. 2a). It exceeds Zn||DB ( $92 \text{ mAh g}^{-1}$ ) and Zn||TA ( $109 \text{ mAh g}^{-1}$ ) cells, implying its excellent charge storage capability. Cyclic voltammogram (CV) profiles of Zn||TNB cell at various scan rates of 1–10  $\text{mV s}^{-1}$  show three pairs of redox peaks (marked as  $P_{R1}$ ,  $P_{R2}$ ,  $P_{R3}$ ,  $P_{O1}$ ,  $P_{O2}$ , and  $P_{O3}$ , Fig. 2b), unveiling the electrochemical reversibility and triple-redox behavior of TNB cathode with an average discharge voltage of 0.9 V. Furthermore, compared with Zn||DB and Zn||TA cells, Zn||TNB battery achieves highly reversible capacities and excellent rate metrics at 0.2–100  $\text{A g}^{-1}$  (Fig. 2c, Fig. S14 and Table S1), highlighting the multi-redox nonplanar structure advantage of TNB. Impressively, high-capacity-voltage TNB cathode endows Zn||TNB battery with a desirable energy output of  $385 \text{ Wh kg}^{-1}_{\text{TNB}}$  (Fig. S15a

and b), which holds potentials to compete with recently reported organic materials used for aqueous batteries (Fig. 2d and Table S2).<sup>7,11,22,38,62–67</sup>

Zn||TNB battery displays stable capacities after 10,000 cycles at  $1 \text{ A g}^{-1}$  (Fig. S16), reflecting the desirable electrochemical reaction process and the intrinsic structural stability of TNB cathode. It also shows superb stability with 84.1% capacity retention over 180,000 cycles at  $10 \text{ A g}^{-1}$  (Fig. 2e and Fig. S16b), surpassing the batteries assembled by DB (15.4%) and TA (76.8%) cathodes. By leveraging the synergistic advantages of planar DB (high activity) and nonplanar TA (low energy barrier and insolubility) while compensating for their respective shortcomings, two rotating tert-N linkages bring the extended nonplanar  $\pi$ - $\pi$  stacking configuration of TNB. This delocalizes excess charges throughout the skeleton and suppresses TNB- $H_2O$  interactions, thereby ensuring structural robustness and excellent anti-dissolution to enable a state-of-the-art cycling lifespan of 180,000 cycles for aqueous zinc batteries (Fig. 2e). To our best knowledge, such a top-class cycling lifespan sets a new record for organic cathode materials in aqueous batteries (Fig. 2f and Table S2).<sup>7,16,27,35,40,49,55,60,62,66,68–74</sup> SEM images, FI-IR spectra and UV-Vis spectra of TNB cathode after long-term cycles prove its structure robustness and anti-dissolution in  $ZnSO_4/H_2O$  electrolyte (Fig. S17), which is responsible for ultradurable Zn||TNB battery (Fig. S18). Besides, the battery delivers highly competitive



capacity of 335 mAh g<sup>-1</sup> (Fig. S19 and Table S3) based on 12.7 mg cm<sup>-2</sup> TNB cathode, displaying the feasibility of Zn-nitroarene batteries as one of the prospective energy storage solutions.

To date, almost all reported ZOBs with high energy densities are typically estimated based on the active organic materials in the cathode.<sup>12,22,27,47,61</sup> For a more comprehensive comparison, when considering the total mass of TNB cathode, consumable Zn anode, and ZnSO<sub>4</sub> electrolyte, Zn||TNB battery still delivers an energy density of 160 Wh kg<sup>-1</sup> cell (Fig. S15c), which holds great potential to compete with a recently reported value (105.1 Wh kg<sup>-1</sup> cell).<sup>75</sup> The excellent comprehensive electrochemical performances of TNB in terms of rate capacity, energy density and cyclic stability make it a promising cathode material for advanced ZOBs. These results also confirm the high compatibility between Zn anode and TNB cathode, which points to a new paradigm for developing advanced ZOBs.

To rationalize the significant performance differences between DB, TA and TNB cathodes in ZOBs, we further studied their interfacial redox processes and charge storage kinetics. The activation energy ( $E_a$ ) of interfacial redox processes of TNB can be revealed via fitting electrochemical impedance spectra (EIS, Fig. S20) based on the relationship between charge transfer resistance ( $R_{ct}$ ) and temperature ( $T$ ). The  $E_a$  value for extended nonplanar TNB is 0.23 eV (Fig. 2g), which is much lower than those of planar DB (0.43 eV) and nonplanar TA (0.30 eV). By circumventing the Coulomb repulsion associated with single-ion hosting in unipolar

organics,<sup>76</sup> the co-storage of Zn<sup>2+</sup> and SO<sub>4</sub><sup>2-</sup> cation/anion activates proton-like low-activation-energy interfacial redox reactions, affording efficient energy storage in TNB cathode. It shows that the nonplanar configuration of TNB can activate fast interfacial redox reaction to fully access redox-active groups in TNB cathode.

Moreover, the linear relationship between the real part of impedance ( $Z'$ ) of EIS and the reciprocal of the square root of angular frequency ( $\omega^{-0.5}$ ) was fitted to gain the ionic diffusion resistance ( $\sigma$ ).<sup>20</sup> Among the three organics, TNB delivers the lowest  $\sigma$  value of 6.8  $\Omega$  s<sup>-0.5</sup> (Fig. 2h), revealing fast ion transport for achieving high-power Zn||TNB cell. Thanks to the  $\pi$ -conjugated nonplanar steric structure, TNB allows for the full exposure of quadruple nitro sites and dual tert-N species, coordinating with Zn<sup>2+</sup> and SO<sub>4</sub><sup>2-</sup> with low energy barriers. Based on Dunn's method,<sup>49,70</sup> the six oxidation-reduction peaks of CV profiles (Fig. 2b) display high  $b$  values of 0.93–0.99 (Fig. 2i), signifying the surface-dominant capacitive charge storage of TNB cathode accompanied by the slight diffusion-limited process (Fig. S21a). Based on galvanostatic intermittent titration technique (GITT), TNB cathode achieves a high ion diffusion coefficient ( $D$ ) with an average value of 10<sup>-8</sup> cm<sup>2</sup> s<sup>-1</sup> (Fig. S21b). These results reveal the high-kinetics and stable energy storage behavior of TNB, which originates from its nonplanar extended conjugation and low-steric-barrier redox-active structure, making for full utilization of ambipolar active motifs and rapid ion migration.

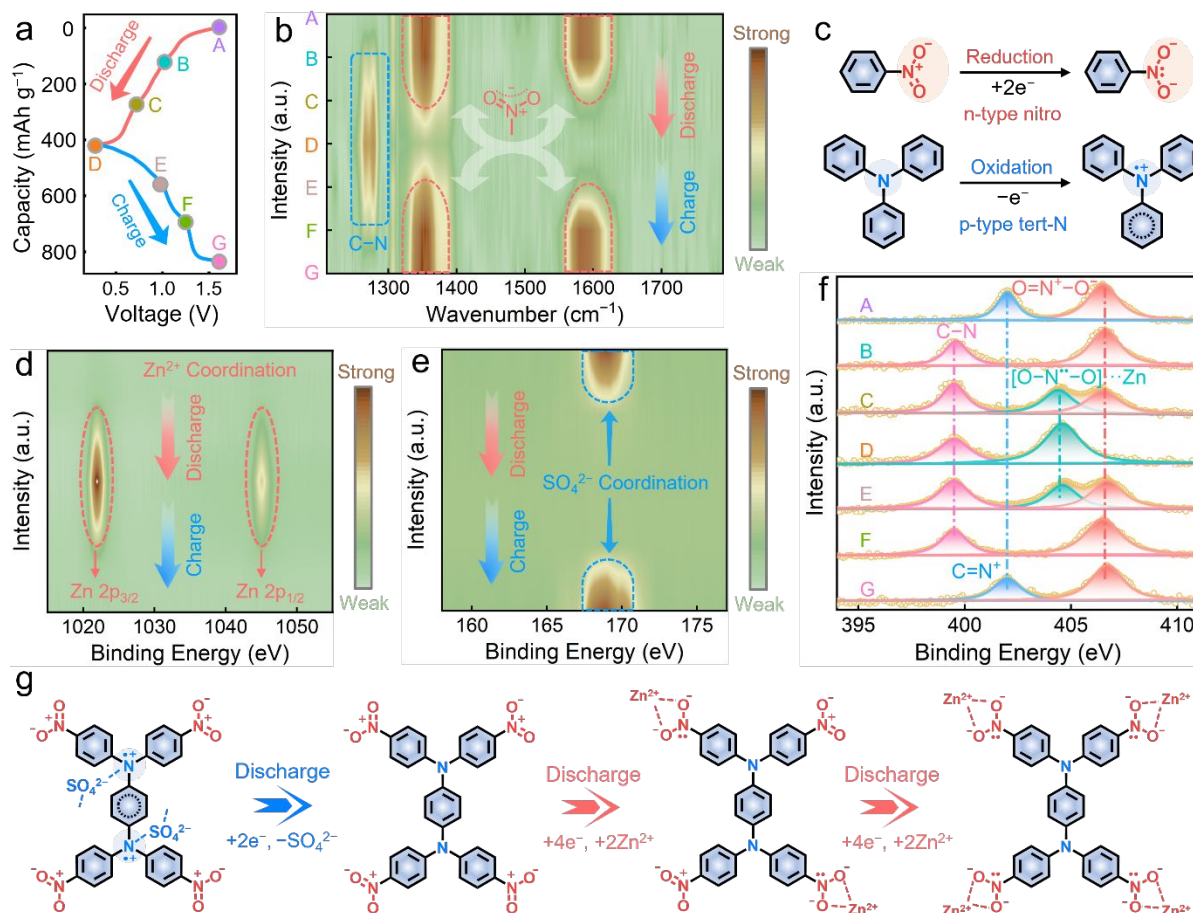


**Fig. 3** Structural evolution of TNB cathode during the operation of Zn||TNB battery. (a) A capacity-potential curve. (b) Overview of FT-IR spectra at the marked points in GCD profile. (c) Redox mechanisms of n-type nitro and p-type tert-N groups. *Ex-situ* XPS spectra of (d) Zn 2p, (e) S 2p, and (f) N 1s. (g) Anion-cation redox storage mechanism.



Encouraged by the outstanding electrochemical metrics of TNB cathode, its charge storage mechanism in ZOBs was analyzed *via* FT-IR spectra and X-ray photoelectron spectroscopy (XPS) characterizations. Seven (dis)charged markers (A, B, C, D, E, F, and G) of the GCD profile of Zn||TNB cell at 0.2 A g<sup>-1</sup> were collected to reveal the redox process of TNB (Fig. 3a). In the 2D contour map of FT-IR spectra (Fig. 3b), two characteristic peaks at 1587 and 1352 cm<sup>-1</sup> (state A) can be ascribed to the stretching vibration of the stretching vibration of the nitro group.<sup>50</sup> The nitro signal remains almost unchanged during discharge (state A→B) and gradually weakens after further discharge proceeding (state B→C→D), implying its n-type reaction activity for the uptake of cationic carriers in the low-potential region. On the contrary, the peak signal of C–N species at 1272 cm<sup>-1</sup> appears (state A→B),<sup>69</sup> and keeps constant during subsequent discharge (state B→C→D), verifying its p-type redox activity for the removal of SO<sub>4</sub><sup>2-</sup> anions in the high-potential area. In the following recharging process (state D→E→F→G), all adsorption signals exhibit opposite trends due to the release of Zn<sup>2+</sup> ions from nitro sites and the uptake of SO<sub>4</sub><sup>2-</sup> anions at tert-N centers. Thus, n-type nitro and p-type tert-N groups of TNB are identified as ambipolar redox-active motifs to afford reversible (de)coordination reactions with fused anion–cation storage (Fig. 3c).

XPS spectra analysis was performed on Zn 2p and S 2p signals to monitor the changes of Zn<sup>2+</sup> cations and SO<sub>4</sub><sup>2-</sup> anions in TNB cathode during a discharge-charge cycle (Fig. 3d and e). During the discharge process (state B→C→D), the Zn 2p signal gradually increases due to Zn<sup>2+</sup> coordination and decreases after charging (state

D→E→F) by Zn<sup>2+</sup> removal (Fig. 3d). On the contrary, S 2p signal exhibits obvious decrease after discharging (state A→B) and reverts to the initial state in the following recharging process (state F→G, Fig. 3e). These results indicate the reversible (de)coordination of SO<sub>4</sub><sup>2-</sup> and Zn<sup>2+</sup> ions. Of note, given the moderately acidic ZnSO<sub>4</sub>/H<sub>2</sub>O solution (pH≈4.4) and the small-sized solvated H<sup>+</sup> ions, identifying whether H<sup>+</sup> serves as the charge carrier is also essential (Fig. S22). Zn||TNB battery using H<sub>2</sub>SO<sub>4</sub>/H<sub>2</sub>O electrolyte (pH≈4.4) delivers a low capacity of 8 mAh g<sup>-1</sup> (Fig. S22a), suggesting the negligible contribution of protons in electrochemical reactions. The lack of flake zinc hydroxide also excludes the participation of protons in discharged TNB cathode (Fig. S22b). Besides, there is no UV-Vis absorption signal for fully reduced TNB cathode in ZnSO<sub>4</sub>/H<sub>2</sub>O electrolyte (Fig. S22c), indicating its robust structure during the electrochemical reaction process.

Furthermore, high-resolution N 1s XPS spectra were analyzed to further unravel the redox behaviors of TNB cathode during battery operation (Fig. 3f). A deconvoluted peak at 402.0 eV can be attributed to C=N<sup>+</sup> species formed at state A, confirming the p-type redox activity of C–N groups. During discharge (state A→B), C=N<sup>+</sup> moieties disappear accompanied by the generation of C–N groups because of the liberation of SO<sub>4</sub><sup>2-</sup> ions (state B→C→D), proving the redox reactions between C–N sites and SO<sub>4</sub><sup>2-</sup> anions in the high-potential region. The rearrangement of C–N covalent bonds into C=N<sup>+</sup> species indicates SO<sub>4</sub><sup>2-</sup>-driven redox reactions (Fig. 3f), rather than physisorption or electrolyte-related artifacts. In contrast, NO<sub>2</sub> motifs at 406.5 eV gradually decrease by taking part in the reduction

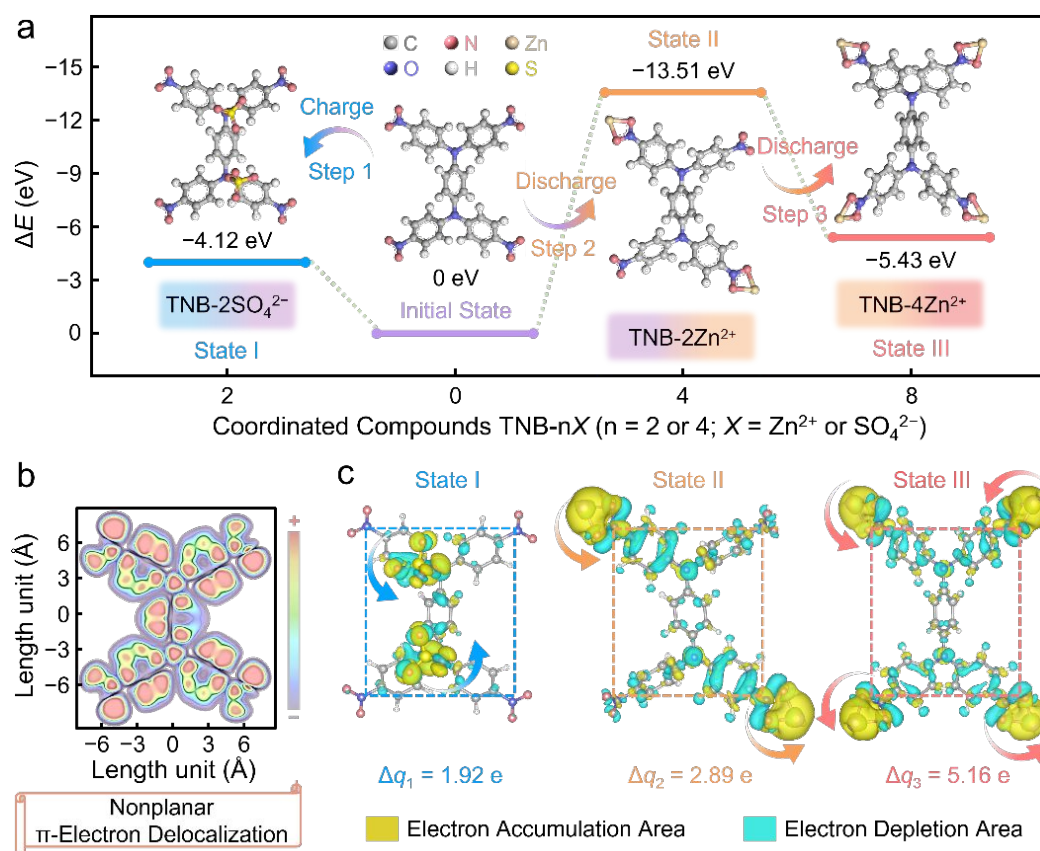


**Fig. 4** Theoretical calculation of stepwise 10 e<sup>-</sup> anion-cation redox reaction of TNB cathode. (a) Optimized geometries and corresponding  $\Delta E$  values after the uptake of opposite charge carriers. (b) ELF- $\pi$  map of TNB. (c) Charge density difference isosurfaces and corresponding Bader charges.



reaction during the low-potential discharging process (state B→C→D) to form  $[O-N^{\bullet}-O] \cdots Zn$  moieties at 404.5 eV. During the recharge process (state D→E→F→G), all signals achieve reversible evolution owing to  $Zn^{2+}$  decoordination from n-type nitro motifs and the uptake of  $SO_4^{2-}$  anions at p-type tert-N sites. Overall, FT-IR spectra (Fig. 3b), and XPS spectra (Fig. 3d–f) confirm the reversible multi-redox utilization of nitro and tert-N groups. The structural change of  $NO_2$  and C–N moieties in TNB cathode agrees with  $NO_2$  groups in DB cathode and C–N groups in TA cathode (Fig. S23). It is worth noting that nitroarenes may be converted into amino compounds via  $H^+$ -coupled irreversible multielectron reduction.<sup>77</sup> Evidently, nitro motifs of TNB cathode are not converted into amine species in slightly acidic  $ZnSO_4/H_2O$  electrolyte (Fig. S24), thus affording highly reversible  $Zn^{2+}$  (de)coordination process.

Spectral results demonstrate the ambipolar charge storage behavior of TNB with alternating reaction of contrary ionic carriers in multisite motifs, entailing  $SO_4^{2-}$ -coupled tert-N redox in the high-potential range and  $Zn^{2+}$ -coupled nitro redox in the low-voltage domain (also confirmed by GCD results, Figs. S25, S26, and S27). The cation/anion co-storage redox mechanism of TNB cathode can be also observed in aqueous  $Zn(OTf)_2$  and  $ZnCl_2$  electrolytes, highlighting its broad electrochemical compatibility across different aqueous electrolytes (Fig. S28). The experimental capacity of TNB cathode is 430  $mAh\ g^{-1}$  (Fig. 2a), which is close to its theoretical value of 452  $mAh\ g^{-1}$ , corresponding to  $\approx 10\ e^-$  redox charge storage process involving four 2  $e^-$  nitro groups and two 1  $e^-$  tert-N groups. By harnessing the synergistic merits of planar DB (multielectron nitro redox) and nonplanar TA (low energy barrier and structural insolubility), two rotating tert-N linkages afford the extended  $\pi$ -aromatic nonplane structure of TNB, which thus fully exposes redox-active nitro/tert-N motifs to allow for 98.9% utilization with a low activation energy of 0.23 eV (vs. 0.43 eV of DB and 0.30 eV of TA, Fig. 2g) via co-storing  $Zn^{2+}$  and  $SO_4^{2-}$  ions (Fig. 3b–f), giving excellent electrochemical activity and stability.

A pouch battery ( $4 \times 4\ cm^2$ ) composed of TNB cathode (12.5  $mg\ cm^{-2}$ ), Zn anode and 3 M  $ZnSO_4/H_2O$  electrolyte was further assembled to evaluate its long-term cycling stability. The battery delivers a high capacity of 178  $mAh\ g^{-1}$  after 3,000 cycles at 10  $A\ g^{-1}$  with 95.2% capacity retention (Fig. S29). Meanwhile, two pouch batteries in series can power a lamp plate (insert of Fig. S29), demonstrating the bright practical prospect. Overall, spectral characterization (Fig. 3a–f, Figs. S23 and S24) and electrochemical analysis (Figs. S22 and S25) reveal that TNB cathode starts a consecutive three-step 10  $e^-$  ambipolar redox reaction (Fig. 3g). It corresponds to the three pairs of redox peaks observed in CV profiles (Fig. 2b), where the voltage gap (0.40 V) between the anion-active and cation-active plateaus is comparable to previously established bipolar systems (0.30–0.38 V).<sup>32,74</sup> The process involves an initial 2  $e^-$  tert-N redox with two  $SO_4^{2-}$  anions ( $P_{O1}/P_{R1}$ ), followed by two-continuous 8  $e^-$  nitro bipedal-coordination with four  $Zn^{2+}$  ions ( $P_{O2}/P_{R2}$  and  $P_{O3}/P_{R3}$ ). TNB overcomes the barriers of structural instability and high redox energy barriers in ever reported organic small molecules, affording excellent performance metrics for state-of-the-art ZOBs (Table S2).

To unravel the electrochemical redox behaviors of TNB, theoretical calculation was further conducted to simulate its molecular structure evolution during battery operation.<sup>78,79</sup> In the optimal TNB

structure,  $Zn^{2+}$  cation coordinated with two oxygen motifs of nitro motif and  $SO_4^{2-}$  anion bound to tert-N site are thermodynamically the most stable coordination geometries (Fig. S30). According to the minimum energy rule, the optimized anion-cation coordination structures of TNB were imitated, which proves the stable three-step continuous 10  $e^-$  redox reaction pathway. In the charge process (step 1), the bind energy ( $\Delta E$ ) demanded for  $SO_4^{2-}$  anions to combine with tert-N sites of pristine TNB is  $-4.12\ eV$  (Fig. 4a and Fig. S31), which forms the anion-doped TNB- $SO_4^{2-}$  complex (state I). In the subsequent discharge process, TNB starts a two-step reduction reaction, in which two  $Zn^{2+}$  cations first couple with two diagonal nitro groups (step 2), and then the other two  $Zn^{2+}$  cations coordinate with the residual two nitro motifs (step 3). The needed  $\Delta E$  values for step 2 and step 3 are  $-13.51$  and  $-5.43\ eV$ , respectively, promoting the formation of cation-coordinated TNB- $2Zn^{2+}$  (state II) and TNB- $4Zn^{2+}$  (state III) products. As a consequence, the favorable anion-cation binding environment promises the rapid and stable multielectron reaction process of TNB cathode in ZOBs.

The electron structure and molecular conjugation effect of TNB was unraveled by the  $\pi$ -electron localization function (ELF- $\pi$ ) calculation.<sup>55</sup> The interconnected ELF- $\pi$  isosurfaces in TNB skeleton show highly nonplane  $\pi$ -aromaticity and  $\pi$ -electron delocalization along the extended conjugation structure (Fig. 4b). The charge-density difference iso-surface analysis,<sup>80</sup> was conducted to deeply untangle redox natures of ion-coupled TNB complex (Fig. 4c). The charge accumulation/consumption around tert-N/nitro regions and ionic carriers can be monitored, unravelling their strong redox interactions to yield robust geometries. This can be also confirmed by obvious Bader charge transfers of 1.01 e (state I), 3.07 e (state II) and 6.19 e (state III), implying the high redox activity of tert-N motifs and nitro moieties. The alternate storage of opposite ions ( $SO_4^{2-}$  anions and  $Zn^{2+}$  cations) allows the utmost utilization of multi-redox nitro/tert-N sites in TNB, giving powerful electrochemical activity and stability.

To demonstrate the electrochemical universality of nonplanar molecular engineering, various multi-redox nonplanar organic small molecules are demonstrated (Fig. 5a–c), including 5,5'-(phenazine-5,10-diyl)diisophthalic acid (PNA), 4,4',4'',4'''-pyrrolo[3,2-b]pyrrole-1,2,4,5(4H)-tetrayltetrakis[benzotrile] (PPT), and N1,N1,N3,N3,N5,N5-hexa(pyridin-4-yl)benzene-1,3,5-triamine (HBT) (Fig. S32). Potential energy curves show that the intramolecular  $\pi$ - $\pi$  interactions between adjacent nonplanar structures of three molecules are stronger than the solvation interaction between  $H_2O$  molecules and organics (Fig. 5d–f). Specifically, compared to the repulsive solvation forces caused by  $H_2O$  molecules, PNA, HBT, and PPT compounds deliver the most negative  $E$  values of  $-21.2$ ,  $-34.5$  and  $-45.6\ kcal\ mol^{-1}$  at the stacked layer  $R$  of 0.31, 0.33, and 0.34 nm, respectively. Such a result indicates strong intramolecular  $\pi$ - $\pi$  forces of PNA, HBT, and PPT, which are expected to achieve excellent anti-dissolution in aqueous electrolytes.

As a proof of concept, PNA, HBT, and PPT were applied as cathodes to couple with Zn metal anodes for building ZOBs. Impressively, all three ZOBs achieve ultradurable electrochemical activity with an extraordinary lifespan of 180,000 cycles at 10  $A\ g^{-1}$ , delivering 71.3%/80.6%/85.1% capacity retentions (Fig. 5g–i), respectively. To reveal the potential dissolution behavior of redox species in aqueous electrolytes, three cathodes at different cycles were



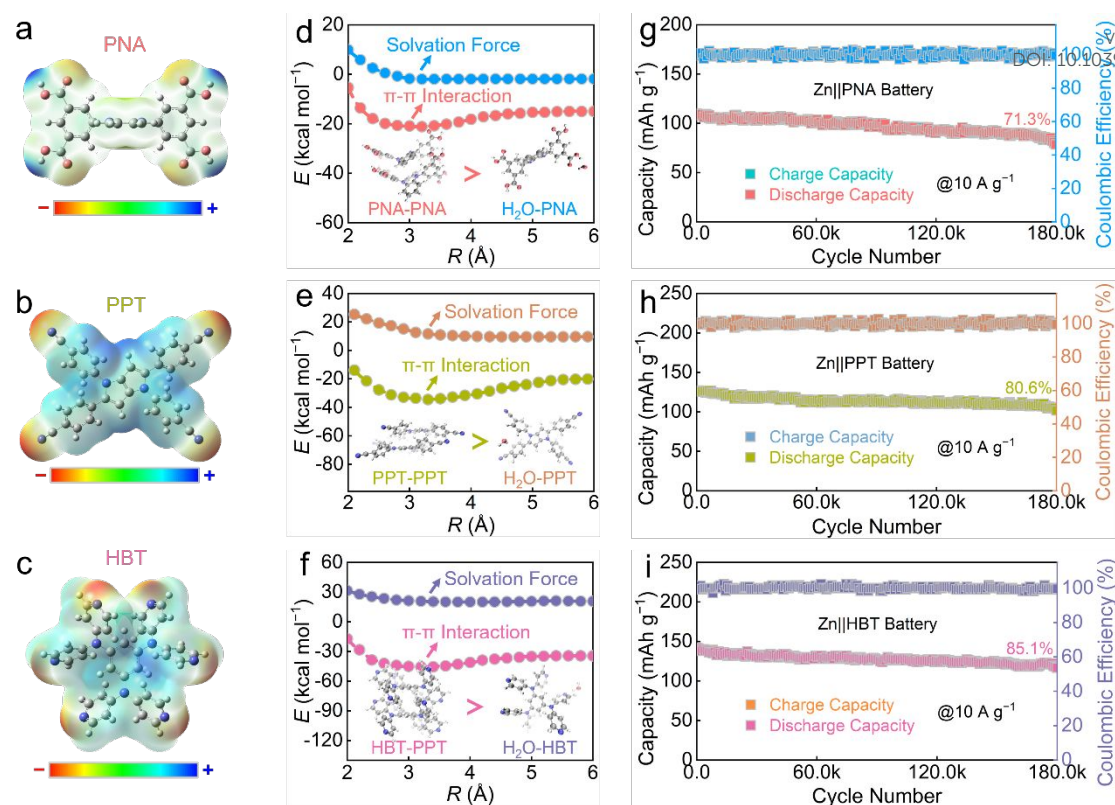


**Fig. 5** (a–c) Molecule structures of three-type organic compounds. (d–f) Potential energy profiles for  $\pi$ - $\pi$  stacked organic molecules in comparison to interacted H<sub>2</sub>O molecules. (g–i) Cycling stability of three organic cathodes in aqueous ZnSO<sub>4</sub> electrolyte.

immersed in aqueous ZnSO<sub>4</sub> electrolytes. There is no absorption signal in UV/Vis spectra (Fig. S33), confirming the structural stability and anti-dissolution of these nonplanar molecules. These results show the great potential of nonplanar small-molecule cathodes in the development of superstable aqueous ZOBs.

Overall, the demonstrated nonplanar tertiary-N extended molecular structure provides a promising platform for developing insoluble and low-energy-barrier organic small molecules towards better aqueous batteries. Preliminary evidence from carboxylic, cyano, and imine derivatives supports the potential transferability of this design strategy, though further systematic optimization is needed to establish it as a universal principle. Key features include: i) High weight content proportions of redox-active aromatic motifs with strong intramolecular  $\pi$ - $\pi$  interactions liberate anti-dissolution in aqueous electrolytes; ii) Rotating tert-N extended  $\pi$ -conjugated skeletons form nonplanar molecular conformations to efficiently access exposed redox-motifs with low energy barriers. More exciting progress can be expected to enrich the organic nonplanar structure library to promote the quest for ever-increasing performances in energy storage communities.

## Conclusion

In conclusion, a nonplanar multi-site-redox TNB cathode with dual-electron-donating rotational tert-N sites and quadruple two-electron-accepting nitro groups is demonstrated, as a new-type cathode material for activating ultrastable ZOBs. We harness the strong intramolecular  $\pi$ - $\pi$  interaction (exceeding the H<sub>2</sub>O dissociation energy in aqueous electrolytes) to inhibit dissolution of the nitroarene

cathode. The extended nonplanar conjugated structure of TNB allows full accessibility of low-steric-barrier nitro and tert-N redox-sites with low energy barriers, and more importantly, promises insolubility in aqueous electrolytes to push the cycle lifespan of ZOBs to a record level. Systemic investigations suggest the 2 e<sup>-</sup> tert-N redox for SO<sub>4</sub><sup>2-</sup> anion storage and 8 e<sup>-</sup> nitro reactions for Zn<sup>2+</sup> cation storage in TNB cathode, liberating superior capacity and large-current survivability. Besides, the nonplanar structure design is transferable to the development of other insoluble redox-active compounds, as exemplified by carboxylic, cyano, and imine derivatives. These proof-of-concept results suggest that this strategy may inspire further exploration of nonplanar molecular engineering for ZOBs. This study paves a new path to develop various nitroaromatic materials and other potential insoluble low-energy-barrier organic molecules to achieve superstable cycles without sacrificing capacity, which would inspire more related nonplanar structure investigations of high-performance organic materials towards advanced energy storage.

## Author contributions

Z.Y.S. conceived the idea, designed the project, and wrote the original paper. M.X.L. supervised the research and revised the paper. Z.Y.S., L.H.G., and Y.K.L. performed the data processing and analysis. Q.H. performed the theoretical simulations. Z.Y.S. and M.X.L. contributed to the manuscript review. All authors engaged in discussions related to the manuscript.

## Conflicts of interest



The authors declare no conflict of interest.

## Acknowledgements

This work is financially supported by the National Natural Science Foundation of China (No. 22309134, 22272118, and 22172111), the Shanghai Rising-Star Program (23YF1449200), the Zhejiang Provincial Science and Technology Project (2022C01182), and the Fundamental Research Funds for the Central Universities.

## Notes and References

- C. Li, D.-D. Wang, G. S. H. P. Ho, Z. Zhang, J. Huang, K.-T. Bang, C. Y. Lau, Sh.-Y. Leu, Y. Wang and Y. Kim, *J. Am. Chem. Soc.*, 2023, **145**, 24603-24614.
- D. J. Kim, D.-J. Yoo, M. T. Otley, A. Prokofjevs, C. Pezzato, M. Owczarek, S. J. Lee, J. W. Choi and J. F. Stoddart, *Nat. Energy*, 2018, **4**, 51-59.
- M. Yu, N. Chandrasekhar, R. K. M. Raghupathy, K. H. Ly, H. Zhang, E. Dmitrieva, C. Liang, X. Lu, T. D. Kühne, H. Mirhosseini, I. M. Weidinger and X. Feng, *J. Am. Chem. Soc.*, 2020, **142**, 19570-19578.
- J. C. Russell, V. A. Posey, J. Gray, R. May, D. A. Reed, H. Zhang, L. E. Marbella, M. L. Steigerwald, Y. Yang, X. Roy, C. Nuckolls and S. R. Peurifoy, *Nat. Mater.*, 2021, **20**, 1136-1141.
- S. Chang, J. F. F. Gomez, S. Katiyar, G. Morell and X. Wu, *J. Am. Chem. Soc.*, 2023, **145**, 24746-24754.
- K. W. Nam, H. Kim, Y. Beldjoudi, T.-w. Kwon, D. J. Kim and J. F. Stoddart, *J. Am. Chem. Soc.*, 2020, **142**, 2541-2548.
- H. Lv, Z. Wei, C. Han, X. Yang, Z. Tang, Y. Zhang, C. Zhi and H. Li, *Nat. Commun.*, 2023, **14**, 3117.
- S. Zhang, Y.-L. Zhu, S. Ren, C. Li, X.-B. Chen, Z. Li, Y. Han, Z. Shi and S. Feng, *J. Am. Chem. Soc.*, 2023, **145**, 17309-17320.
- Y. Mu, J. Nyakuchena, Y. Wang, J. R. Wilkes, T. Luo, M. Goldstein, B. Elander, U. Mohanty, J. L. Bao, J. Huang and D. Wang, *Angew. Chem. Int. Ed.*, 2024, **63**, e202409286.
- J. Yan, B. Wang, Y. Tang, W. Du, M. Ye, Y. Zhang, Z. Wen, X. Liu and C. C. Li, *Angew. Chem. Int. Ed.*, 2024, **63**, e202400121.
- Z. Tie, Y. Zhang, J. Zhu, S. Bi and Z. Niu, *J. Am. Chem. Soc.*, 2022, **144**, 10301-10308.
- S. Li, J. Shang, M. Li, M. Xu, F. Zeng, H. Yin, Y. Tang, C. Han and H. M. Cheng, *Adv. Mater.*, 2023, **35**, 2207115.
- Z. Xu, M. Li, W. Sun, T. Tang, J. Lu and X. Wang, *Adv. Mater.*, 2022, **34**, 2200077.
- Z. Jin, Q. Cheng, S. T. Bao, R. Zhang, A. M. Evans, F. Ng, Y. Xu, M. L. Steigerwald, A. E. McDermott, Y. Yang and C. Nuckolls, *J. Am. Chem. Soc.*, 2022, **144**, 13973-13980.
- X. Guo, P. Apostol, X. Zhou, J. Wang, X. Lin, D. Rambabu, M. Du, S. Er and A. Vlad, *Energy Environ. Sci.*, 2024, **17**, 173-182.
- Q. Q. Sun, T. Sun, J. Y. Du, K. Li, H. M. Xie, G. Huang and X. B. Zhang, *Adv. Mater.*, 2023, **35**, 2301088.
- J. Chu, Z. Liu, J. Yu, L. Cheng, H. G. Wang, F. Cui and G. Zhu, *Angew. Chem. Int. Ed.*, 2023, **63**, e202314411.
- J. Wang, P. Poizot, A. E. Lakranych, X. Liu, L. Sieuw, C. Morari and A. d. Vlad, *Nat. Mater.*, 2023, **20**, 665-673.
- Y. Chen, H. Dai, K. Fan, G. Zhang, M. Tang, Y. Gao, C. Zhang, L. Guan, M. Mao, H. Liu, T. Zhai and C. Wang, *Angew. Chem. Int. Ed.*, 2023, **62**, e202302539.
- Z. Song, L. Miao, H. Duan, L. Ruhlmann, Y. Lv, D. Zhu, L. Li, L. Gan and M. Liu, *Angew. Chem. Int. Ed.*, 2022, **61**, e202208821. DOI: 10.1039/D6EE02250B
- Y. Zhong, Y. Li, J. Meng, X. Lin, Z. Huang, Y. Shen and Y. Huang, *Energy Storage Mater.*, 2021, **43**, 492-498.
- W. Li, H. Xu, H. Zhang, F. Wei, L. Huang, S. Ke, J. Fu, C. Jing, J. Cheng and S. Liu, *Nat. Commun.*, 2023, **14**, 5235.
- L. Lin, Z. Lin, J. Zhu, K. Wang, W. Wu, T. Qiu and X. Sun, *Energy Environ. Sci.*, 2023, **16**, 89-96.
- Z. Tian, V. S. Kale, Y. Wang, S. Kandambeth, J. Czaban-Józwiak, O. Shekhah, M. Eddaoudi and H. N. Alshareef, *J. Am. Chem. Soc.*, 2021, **143**, 19178-19186.
- Q.-Q. Sun, J.-Y. Du, T. Sun, Z.-B. Zhuang, Z.-L. Xie, H.-M. Xie, G. Huang and X.-B. Zhang, *Adv. Mater.*, 2024, **36**, 2313388.
- X. Huang, X. Qiu, W. Wang, J. Li, Z. Li, X. Yu, J. Ma and Y. Wang, *J. Am. Chem. Soc.*, 2023, **145**, 25604-25613.
- L. Lin, Z. Xue, T. Qiu, J. Zhu, G. Zhang, H. Zhan, K. Wang and X. Sun, *Energy Environ. Sci.*, 2024, **17**, 6499-6506.
- J. Zhu, Z. Tie, S. Bi and Z. Niu, *Angew. Chem. Int. Ed.*, 2024, **63**, e202403712.
- S. Zheng, D. Shi, D. Yan, Q. Wang, T. Sun, T. Ma, L. Li, D. He, Z. Tao and J. Chen, *Angew. Chem. Int. Ed.*, 2022, **61**, e202117511.
- Z. Li, J. Tan, Y. Wang, C. Gao, Y. Wang, M. Ye and J. Shen, *Energy Environ. Sci.*, 2023, **16**, 2398-2431.
- H. Peng, S. Huang, V. Montes-García, D. Pakulski, H. Guo, F. Richard, X. Zhuang, P. Samori and A. Ciesielski, *Angew. Chem. Int. Ed.*, 2023, **62**, e202216136.
- N. Wang, Z. Guo, Z. Ni, J. Xu, X. Qiu, J. Ma, P. Wei and Y. Wang, *Angew. Chem. Int. Ed.*, 2021, **60**, 20826-20832.
- C. Zhang, W. Ma, C. Han, L.-W. Luo, A. Daniyar, S. Xiang, X. Wu, X. Ji and J.-X. Jiang, *Energy Environ. Sci.*, 2021, **14**, 462-472.
- P. Yi, Z. Li, L. Ma, B. Feng, Z. Liu, Y. Liu, W. Lu, S. Cao, H. Fang, M. Ye and J. Shen, *Adv. Mater.*, 2024, **36**, 2414379.
- Y. Liu, Y. Lu, A. Hossain Khan, G. Wang, Y. Wang, A. Morag, Z. Wang, G. Chen, S. Huang, N. Chandrasekhar, D. Sabaghi, D. Li, P. Zhang, D. Ma, E. Brunner, M. Yu and X. Feng, *Angew. Chem. Int. Ed.*, 2023, **62**, e202306091.
- S. M. Pallasch, M. Bhosale, G. J. Smales, C. Schmidt, S. Riedel, Z. Zhao-Karger, B. Esser and O. Dumele, *J. Am. Chem. Soc.*, 2024, **146**, 17318-17324.
- L. Yan, Q. Zhu, Y. Qi, J. Xu, Y. Peng, J. Shu, J. Ma and Y. Wang, *Angew. Chem. Int. Ed.*, 2022, **61**, e202211107.
- U. Mittal, F. Colasuonno, A. Rawal, M. Lessio and D. Kundu, *Energy Storage Mater.*, 2022, **46**, 129-137.
- Zhao, Y.; Huang, Y.; Wu, F.; Chen, R. Li, L. Y. Zhao, Y. Huang, F. Wu, R. Chen and L. Li, *Adv. Mater.*, 2021, **33**, 2106469.
- I. Obraztsov, R. Langer, J. G. A. Ruthes, V. Presser, M. Otyepka, R. Zbořil and A. Bakandritsos, *Energy Environ. Sci.*, 2024, **17**, 8874-8884.
- J. Kim, Y. Kim, J. Yoo, G. Kwon, Y. Ko and K. Kang, *Nat. Rev. Mater.*, 2022, **8**, 54-70.
- T. Chen, H. Banda, L. Yang, J. Li, Y. Zhang, R. Parenti and M. Dincă, *Joule*, 2023, **7**, 986-1002.
- S. Meng, T. He, L. Chen, K. Liao, H. Lu, T. Liu, R. Meng, J. Ma, C. Zhang and J. Yang, *Energy Environ. Sci.*, 2024, **17**, 5162-5172.
- D. Du, J. Zhou, Z. Yin, G. Feng, W. Ji, H. Huang and S. Pang, *Adv. Energy Mater.*, 2024, **14**, 2400580.
- W. Li, H. Ma, W. Tang, K. Fan, S. Jia, J. Gao, M. Wang, Y. Wang, B. Cao and C. Fan, *Nat. Commun.*, 2024, **15**, 9533.
- Y. Zhang, Q. Huang, P. Liu, Y. Lv, Z. Song, L. Gan, M. Liu, *Nat. Commun.*, 2026, **17**, 4001.
- Y. Chen, J. Li, Q. Zhu, K. Fan, Y. Cao, G. Zhang, C. Zhang, Y. Gao, J. Zou, T. Zhai and C. Wang, *Angew. Chem. Int. Ed.*, 2022, **61**, e202116289.



48. S. Gaber, A. K. Mohammed, B. H. Javaregowda, J. I. Martínez, P. P. Sánchez, F. Gándara, K. Krishnamoorthy and D. Shetty, *Angew. Chem. Int. Ed.*, 2024, **63**, e202409256.
49. F. Ye, Q. Liu, H. Dong, K. Guan, Z. Chen, N. Ju and L. Hu, *Angew. Chem. Int. Ed.*, 2022, **61**, e202214244.
50. X. Liu and Z. Ye, *Adv. Energy Mater.*, 2020, **11**, 2003281.
51. K. Amin, B. C. Baker, L. Pan, W. Mehmood, Z. Hao, R. Nawaz, Z. Wei and C. F. J. Faul, *Adv. Mater.*, 2024, **37**, 2410262.
52. L. Zhong, C. Liu, Y. Zhang, J. Li, F. Yang, Z. Zhang and D. Yu, *Angew. Chem. Int. Ed.*, 2025, **64**, e202413971.
53. J. Wang, X. Guo, P. Apostol, X. Liu, K. Robeyns, L. Gence, C. Morari, J.-F. Gohy and A. Vlad, *Energy Environ. Sci.*, 2022, **15**, 3923-3932.
54. Z. Song, L. Miao, Y. Lv, L. Gan and M. Liu, *Angew. Chem. Int. Ed.*, 2023, **62**, e202309446.
55. T. Sun, W. Zhang, Z. Zha, M. Cheng, D. Li and Z. Tao, *Energy Storage Mater.*, 2023, **59**, 102778.
56. Y. Chen, D. Zhang, Y. Qin, C. Hu, L. Miao, Y. Lv, Z. Song, L. Gan, M. Liu, *Nat. Commun.*, 2026, **17**, 3599.
57. X. Shi, A. Yi, Q. Liu, Y. Zhang, S. Lin and X. Lu, *ACS Nano*, 2023, **17**, 25005-25013.
58. Y. Xiu, A. Mauri, S. Dinda, Y. Pramudya, Z. Ding, T. Diemant, A. Sarkar, L. Wang, Z. Li, W. Wenzel, M. Fichtner and Z. Zhao-Karger, *Angew. Chem. Int. Ed.*, 2022, **62**, e202212339.
59. H. Cui, D. Zhang, Z. Wu, J. Zhu, P. Li, C. Li, Y. Hou, R. Zhang, X. Wang, X. Jin, S. Bai and C. Zhi, *Energy Environ. Sci.*, 2024, **17**, 114-122.
60. W. Du, Y. Zhang, H. Duan, Y. Lv, Z. Song, L. Gan, M. Liu, *Sci. Adv.*, 2026, **12**, eaec9924.
61. W. Sun, F. Zhu, W. Guo and Y. Fu, *J. Am. Chem. Soc.*, 2025, **147**, 5089-5098.
62. X. Ren, D. Tao, S. Cui, T. Li, Y. Cao and F. Xu, *Energy Storage Mater.*, 2023, **63**, 102992.
63. G. Studer, A. Schmidt, J. Büttner, M. Schmidt, A. Fischer, I. Krossing and B. Esser, *Energy Environ. Sci.*, 2023, **16**, 3760-3769.
64. N. Patil, C. de la Cruz, D. Ciurdac, A. Mavrandonakis, J. Palma and R. Marcilla, *Adv. Energy Mater.*, 2021, **11**, 2100939.
65. C. Han, H. Li, Y. Li, J. Zhu and C. Zhi, *Nat. Commun.*, 2021, **12**, 2400.
66. L. Zhong, C. Liu, Y. Zhang, J. Li, F. Yang, Z. Zhang and D. Yu, *Joule*, 2023, **7**, 971-985.
67. W. Wang, V. S. Kale, Z. Cao, Y. Lei, S. Kandambeth, G. Zou, Y. Zhu, E. Abouhamad, O. Shekhah, L. Cavallo, M. Eddaoudi and H. N. Alsharief, *Adv. Mater.*, 2021, **33**, 2103617.
68. F. Qiao, J. Wang, R. Yu, M. Huang, L. Zhang, W. Yang, H. Wang, J. Wu, L. Zhang, Y. Jiang and Q. An, *ACS Nano*, 2023, **17**, 23046-23056.
69. L. W. Luo, C. Zhang, W. Ma, C. Han, X. Ai, Y. Chen, Y. Xu, X. Ji and J. X. Jiang, *Adv. Mater.*, 2024, **36**, 2406106.
70. L. Xie, K. Xu, W. Sun, Y. Fan, J. Zhang, Y. Zhang, H. Zhang, J. Chen, Y. Shen, F. Fu, H. Kong, G. Wu, J. Wu, L. Chen and H. Chen, *Angew. Chem. Int. Ed.*, 2023, **62**, e202300372.
71. Y. Lin, H. Cui, C. Liu, R. Li, S. Wang, G. Qu, Z. Wei, Y. Yang, Y. Wang, Z. Tang, H. Li, H. Zhang, C. Zhi and H. Lv, *Angew. Chem. Int. Ed.*, 2023, **62**, e202218745.
72. C. Wang, R. Li, Y. Zhu, Y. Wang, Y. Lin, L. Zhong, H. Chen, Z. Tang, H. Li, F. Liu, C. Zhi and H. Lv, *Adv. Energy Mater.*, 2023, **14**, 2302495.
73. X. Peng, Y. Xie, A. Baktash, J. Tang, T. Lin, X. Huang, Y. Hu, Z. Jia, D. J. Searles, Y. Yamauchi, L. Wang and B. Luo, *Angew. Chem. Int. Ed.*, 2022, **61**, e202203646.
74. Z. Song, Q. Huang, Y. Lv, L. Gan and M. Liu, *Angew. Chem. Int. Ed.*, 2025, **64**, e202418237.
75. Y. Zhang, M. Li, Z. Li, Y. Lu, H. Li, J. Liang, X. Hu, L. Zhang, K. Ding, Q. Xu, H. Liu and Y. Wang, *Angew. Chem. Int. Ed.*, 2025, **64**, e202416542.
76. W. Sun, C. Zhou, Y. Fan, Y. He, H. Zhang, Z. Quan, H. Kong, F. Fu, J. Qin, Y. Shen and H. Chen, *Angew. Chem. Int. Ed.*, 2023, **62**, e202300158.
77. Z. Chen, H. Su, P. Sun, P. Bai, J. Yang, M. Li, Y. Deng, Y. Liu, Y. Geng and Y. Xu, *Proc. Natl. Acad. Sci. USA.*, 2022, **169**, e2116775119.
78. N. Wang, R. Zhou, H. Li, Z. Zheng, W. Song, T. Xin, M. Hu and J. Liu, *ACS Energy Lett.*, 2021, **6**, 1141-1147.
79. J. Yang, H. Hua, H. Yang, P. Lai, M. Zhang, Z. Lv, Z. Wen, C. C. Li, J. Zhao and Y. Yang, *Adv. Energy Mater.*, 2023, **13**, 2204005.
80. H. Lu, J. Hu, K. Zhang, Y. Zhang, B. Jiang, M. Zhang, S. Deng, J. Zhao, H. Pang and B. Xu, *Adv. Mater.*, 2024, **36**, 2408396.



The data that support the findings of this study are available from the corresponding authors upon reasonable request.

[View Article Online](#)

DOI: 10.1039/D6EE02250B

